Fusion Science and Technology

ISSN: 1536-1055 (Print) 1943-7641 (Online) Journal homepage: www.tandfonline.com/journals/ufst20

First Results of the Tritium Absorption InfraRed Spectroscopy (T_2ApIR) Experiment

Alexander Marsteller, Dominic Batzler, Beate Bornschein, Lutz Bornschein, Elisabeth Eckard , Florian Hanß , Joshua Kohpeiß , Daniel Kurz , Ralph Lietzow , Michael Sturm, Tin Vrkic , Stefan Welte & Robin Größle

To cite this article: Alexander Marsteller, Dominic Batzler, Beate Bornschein, Lutz Bornschein, Elisabeth Eckard , Florian Hanß , Joshua Kohpeiß , Daniel Kurz , Ralph Lietzow , Michael Sturm, Tin Vrkic , Stefan Welte & Robin Größle (17 Jun 2026): First Results of the Tritium Absorption InfraRed Spectroscopy (T_2ApIR) Experiment, Fusion Science and Technology, DOI: 10.1080/15361055.2026.2676408

To link to this article: https://doi.org/10.1080/15361055.2026.2676408

FUSION SCIENCE AND TECHNOLOGY

DOI: https://doi.org/10.1080/15361055.2026.2676408

First Results of the Tritium Absorption InfraRed Spectroscopy (T_2ApIR) Experiment

Alexander Marsteller, Dominic Batzler, Beate Bornschein, Lutz Bornschein, Elisabeth Eckard, Florian Hanß, Joshua Kohpeiß, Daniel Kurz, Ralph Lietzow, Michael Sturm, Tin Vrkic, Stefan Welte, and Robin Größle

Institute for Astroparticle Physics, Tritium Laboratory Karlsruhe(IAP-TLK), Karlsruhe Institute of Technology (KIT), Eggenstein-Leopoldshafen, Germany

Received December 19, 2025
Accepted for Publication May 8, 2026

Abstract — *The literature on the experimentally verified material properties of tritium is sparse, but information about this is crucial in fusion for pellet production (magnetic confinement fusion), target fueling (inertial confinement fusion), and cryogenic distillation, as well as in astroparticle physics for neutrino experiments and the search for rare physics.*

To improve on this, the T_2ApIR (Tritium Absorption InfraRed Spectroscopy 2) experiment, designed and built at the Tritium Laboratory Karlsruhe, is in its scientific commissioning phase. The main focus of this experiment is to enable the investigation of the properties of all six hydrogen isotopologues and their mixtures in the gaseous, liquid, and solid phases, as well as the dynamics of their phase changes. In addition, mixtures with noble gases, such as xenon and neon, can be investigated.

This is achieved using a cryogenic setup capable of reaching less than 10 K in a measurement cell that allows for optical access for infrared absorption spectroscopy, Raman spectroscopy, and a polariscope setup, as well as temperature and pressure measurements. Scientific commissioning measurements using the inactive hydrogen isotpologues (H_2, HD, and D_2) have demonstrated these analytical capabilities prior to tritium commissioning of the apparatus.

Keywords — *Tritium Laboratory Karlsruhe, cryogenic tritium, thermodynamical properties of hydrogen isotopologues, Raman spectroscopy, infrared spectroscopy.*

I. INTRODUCTION

Tritium (T and T_2), the radioactive isotope of hydrogen, is of particular interest as an electron source for neutrino mass measurements [1–5] as a natural background and as a calibration source for dark matter search [6–10]. Tritium is also the most promising fuel in fusion for power generation [11].

In the former case, detailed knowledge of the properties of tritium is necessary to accurately determine the uncertainties of the neutrino mass measurement and the design of the tritium electron source. In the latter case, material properties [12] inform the design and feasibility of fuel cycle concepts, including processes such as cryogenic distillation, production of pellets for magnetic confined fusion or targets for laser fusion, and finally, for the development of analytic systems and concepts for monitoring and accountancy.

In general, cold hydrogen isotopologues are of interest in wide fields of research from ortho/para-conversion [13] for hydrogen liquefaction to the production of ultra-cold neutrons and tests of fundamental interactions, like ultra-cold neutrons scattering on cold deuterium [14].

Current research at the Tritium Laboratory Karlsruhe (TLK) focuses on the thermodynamic properties of high-

---

CONTACT Alexander Marsteller alexander.marsteller@kit.edu

purity H-D-T mixtures [12,15–17] and the development of analytical tools [18–22] for target production, pellet production, cryogenic pumping and cryogenic distillation, and water detritiation [23] for inertial and magnetic confined fusion.

In cryogenic distillation for isotope separation, the six hydrogen isotopologues ($Q_2 = T_2$, DT, D_2, HT, HD, and H_2) are separated in a cryogenic distillation column by differences in their vapor pressures at a given temperature. As the highest boiling isotopologue, with a boiling point of 24.99 K at 1 bar [24], tritium (T_2) accumulates at the bottom of the column in the liquid phase. To monitor the concentration of T_2, as well as the residual amounts of HT and DT, a measurement system is required.

Offline methods to measure this concentration, such as gas chromatography, do not allow for a real-time monitoring of a process on the scale of seconds or minutes, requiring measurement times on the many minutes to hour scale with additional sample and waste processing, as well as frequent recalibration [25,26]. At the TLK, infrared (IR) absorption spectroscopy, which is under investigation as an online and inline monitoring tool, has been successfully calibrated for the inactive isotopologues with an accuracy of better than 5% absolute [27,28].

The production of fuel targets for inertial confined fusion for a commercial fusion power plant requires a fast rate (10 Hz [29]) of target production in order to achieve the desired output power while keeping the overall tritium inventory low [30]. A key step in this process is loading targets with a deuterium-tritium mixture and fixing it, for example, via freezing out the tritium.

In order to address these open questions, an experimental setup to calibrate the spectroscopic methods, study the thermodynamic properties, and investigate the dynamic phase-space behavior of all six hydrogen isotopologues Q_2 at cryogenic temperatures at high density is necessary. Such a setup should allow for investigating all six hydrogen isotopologues Q_2 in different phases, mixtures, pressures, and ortho/para states, and at the triple point using IR and Raman spectroscopy, as well as optical analysis. Based on previous experience with the inactive hydrogen isotopologues (H_2, HD, and D_2) [27,31] the Tritium Absorption InfraRed Spectroscopy 2 (T_2ApIR) experiment [32] has been set up and commissioned at the TLK.

In this work, the commissioning results for the dynamic processes for the inactive hydrogen isotopologues (H_2, HD, and D_2) in the T_2ApIR setup are presented. These measurements demonstrate the second-to-minute scale real-time performance of the analytic systems in T_2ApIR.

II. EXPERIMENTAL SETUP

The setup of the T_2ApIR experiment, with a focus on its construction and design decisions, is described in detail in Refs. [32] and [33]. In order to ensure safe operation with tritium, the entire setup is enclosed by a glove box and connected to the TLK closed tritium-loop infrastructure [34].

T_2ApIR consists of a cryogenic sample cell with two sapphire windows for optical access in a transmission configuration. This access can be used for transmission absorption IR spectroscopy, Raman spectroscopy, and backlight photography (with white light, monochrome light, polarized and nonpolarized). A motorized stage enables an automated change between measurement methods, allowing for the quasi-simultaneous measurement of the IR spectra, Raman spectra, and photographs of the cell contents. A schematic depiction of these optical beam paths in the T_2ApIR setup is shown in Fig. 1.

IR spectroscopy is performed using a commercially available Bruker Vertex 70 Fourier-transform infrared (FTIR) spectrometer. Due to the sapphire windows of the cryogenic sample cell, the lower limit of the wavenumber range of the IR spectrum is around 2100 cm^{-1}. The built-in optical components of the spectrometer result in an upper limit of 9000 cm^{-1}. To remove background from atmospheric water, the IR beam path is continuously flushed with nitrogen and further dried with silica gel. The IR interferogram is directed through the cell via mirrors, allowing for both the spectrometer and its detector to reside outside of the glove box, preventing contamination.

For the throughpass Raman spectroscopy system, a TLK-developed micro Raman (μRa) system [18] is used in a forward Raman configuration. The excitation laser light is produced by a rgb lasersystems Lambda Beam 532-nm diode–pumped, solid-state laser with a power of 200 mW. The produced Raman light is analyzed by one of several exchangeable Ocean Insight QePro spectrometers, which allow for the investigation of either the S_0-branch (rotational) or the Q_1-branch (rovibrational) of the hydrogen isotopologues.

Control of the laser and spectrometer, as well as the real-time data analysis of the Raman spectra on a subsecond timescale, is handled by the μRa control software [18]. Both the excitation and the Raman light are guided into/out of the glove box using optical fibers, allowing for both the laser and the spectrometer to reside outside of the glove box, preventing contamination.

Inside of the glove box, a laser cleanup filter before the cell removes excitations from the connecting fiber,

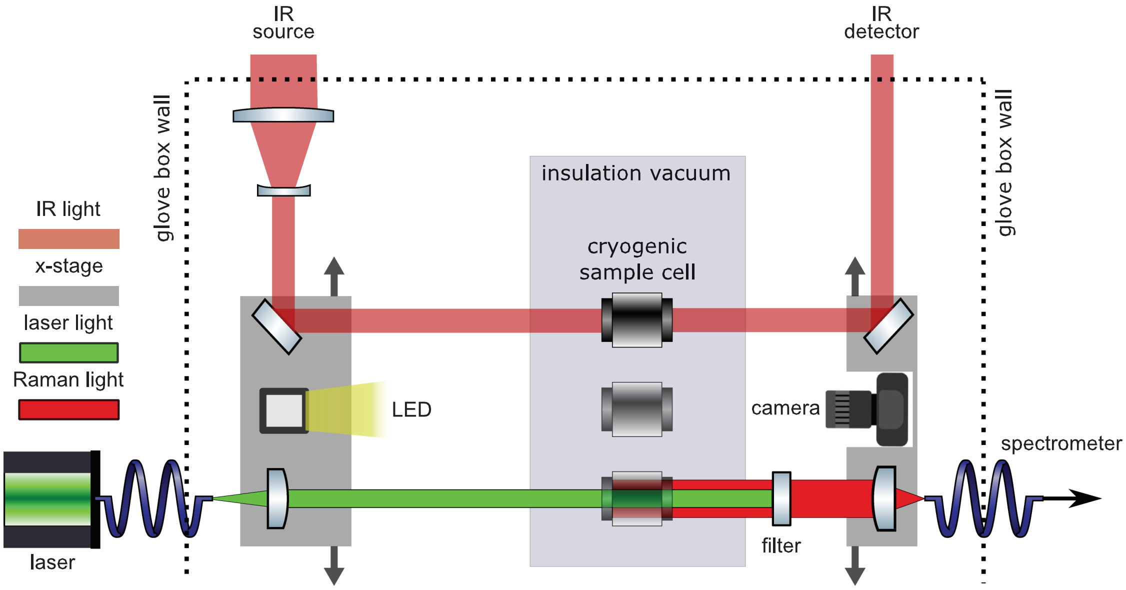

Fig. 1. Experimental idea including the IR system, the throughpass laser Raman system, and photography in a measurement cell. The sample cell is included in the figure multiple times to illustrate the photography and Raman beam path. Only one cell at a fixed position is present in the setup.

while a long-pass filter with a cut-on at 534.4 nm after the cell removes the 532-nm excitation laser light.

For optical investigations, a Canon EOS R system camera with a 100-mm F/2.8 L IS USM macro lens is used to take images and videos of the cryogenic measurement cell.

Additionally, linear polarizers mounted on motorized rotation stages can be inserted on both sides of the measurement cell. This allows for polarization-dependent spectroscopic measurements, as well as for photographic polariscopy. Polariscopy makes it possible to investigate stress inside the solid cell contents via color changes when using white light back-illumination [35] and enhances the contrast of the density fluctuations in the liquid phase.

A short overview of the key cryogenic and spectroscopic performance parameters is given in Table 1.

III. RESULTS

In the following, the first results obtained with the T_2ApIR experiment are presented. First, the optical investigations into the phase change behavior with a focus on crystallization is provided, followed by spectral data with a focus on the dynamic processes.

III.A. Photography-Based Optical Observations of Phase Change

The cryogenic measurement cell of the T_2ApIR experiment can reach the temperatures required to cause hydrogen to liquefy and crystallize. Via the optical windows of the cell, this phase change can be observed with

TABLE 1

Key Performance Parameters of the T_2ApIR Setup

Parameter	Quantity	Value
Temperature	Stability	0.1 K
Pressure	Maximum	2.5 bar
FTIR	Wavenumber range	2100 to 9000 cm^{-1}
	Resolution	0.5 cm^{-1}
Raman	Raman shift range	50 to 2950 cm^{-1}/1000 to 5000 cm^{-1}
	Resolution (full width at half maximum)	9.8 cm^{-1}/16.0 cm^{-1}
	Acquisition time	0.5 to 3600 s

imaging optics, such as a camera using back-illumination from the opposite side of the cell.

An example photograph of the cell filled with a system of solid, liquid, and gaseous protium (H_2) is shown in Fig. 2. The interface between the gaseous phase at the top of the cell and the liquid phase in the middle (region within the cyan dotted line) is visible as a pronounced dark meniscus, which is the result of the light of the back-illumination being refracted away from the optical axis of the camera.

The phase boundary between liquid and solid (region within the red dotted line) is visible as a dark ridge as well due to the boundary not being perpendicular to the cell windows, again refracting light away. In the solid phase, several hairline surface features are visible, with the best contrast close to the phase boundary. The solid is frozen asymmetrically, most likely due to the differences in the thermal resistance between the measurement cell and the cryocooler across the interface between them, which causes a slight temperature gradient across the cell.

III.A.1. Slow Crystal Growth

For a slow crystal growth, two methods were tested and established for H_2 and D_2. One method was the growth via the liquid phase, and the other was desublimation. The latter uses the direct transition from the gaseous to the solid phase. To grow a hydrogen crystal from the liquid, the cell temperature is initially set to a temperature slightly above the triple point of the used hydrogen isotopologue. By condensation, the cell fills up with liquid until the desired fill level is reached. Subsequently, the temperature is reduced slightly below the corresponding triple point. The crystallization then starts at the bottom of the cell, and the crystal grows slowly to the top until the whole liquid is transformed into the solid phase, as can be seen in Fig. 3.

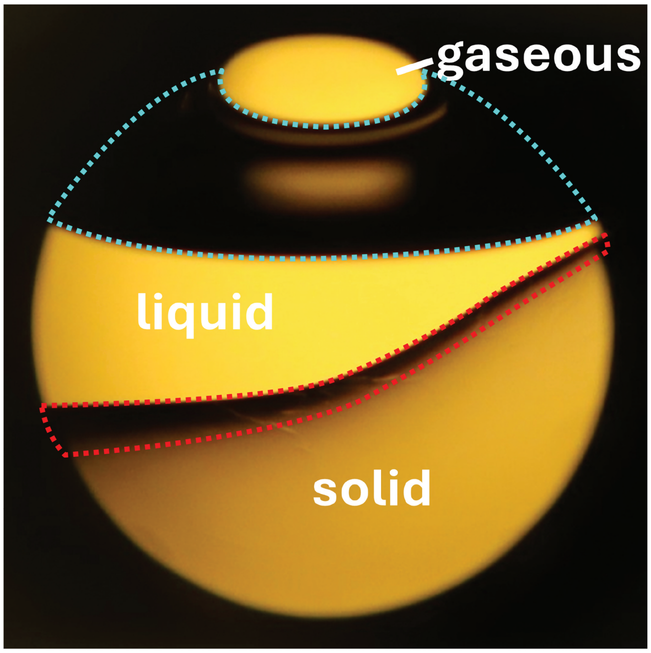

Fig. 2. Photograph of the T_2ApIR measurement cell content. The cell is filled with a system of all three phases of protium (H_2). The cyan dotted line shows the meniscus of the liquid-gas phase boundary. The red dotted line shows the saddle shaped liquid-solid boundary region.

This method results in a directly transparent hydrogen crystal that can then be analyzed, e.g., by IR spectroscopy. However, if the temperature is reduced too far below the triple point, the initially slow crystal growth goes over into a different behavior, as described in Sec. III.A.2. Therefore, the temperature is a very crucial parameter for this method of crystal growth.

To grow a crystal via desublimation, the sample cell is coupled with a buffer vessel filled with the desired hydrogen isotopologue. The initial pressure in this configuration is set to a value below 100 mbar. The exact value is chosen according to the isotopologue's phase diagram. During the process, a slowly growing crystal layer at the lower part of the cell can be observed, which then grows to a crystal filling out the whole sample cell.

During this process, the pressure inside the cell and buffer vessel decreases due to the material deposited in the crystal. The amount of hydrogen in the buffer vessel, however, is large enough to produce a cell-filling crystal. In principle, keeping the pressure constant during the growth process is possible by buffering the buffer vessel directly from the gas supply line. A subsequent annealing phase, therefore, is required before IR spectroscopy is possible.

For both methods, the influence of the pressure and temperature parameters, as well as the corresponding gradients, needs further investigation. So far, both procedures have been performed multiple times with reproducible results.

III.A.2. Rapid Crystal Growth

When deuterium D_2 is cooled down quickly below its freezing point, a different behavior can be seen, as shown in Fig. 4. At first, a spontaneous formation of small nucleation sites along the interfaces of the liquid and the windows can be seen (see e.g., $t = 06$s in the figure). These nucleation sites appear to lose their sharply defined shape quickly (see e.g., $t = 14$ s). Shortly afterward, the

Fig. 3. Slow freezing of liquid H2. The cell was approximately 90% filled at the beginning of the shown process. The temperature of the cell during freezing was slightly below ≈14 K with the pressure gradually decreasing to 0.074 bar. Images are sequentially from left to right, then top to bottom. The entire sequence of images depicts a time span of ≈100 min.

formation of a crystal structure in the bulk liquid can be seen (starting at $t = 18$ s), which continues until the entire liquid phase is crystallized.

After remaining in this state for a short period of time, the formation of what appear to be fronts of phase change traveling across the solid can be observed (starting at $t = 24$ s). These fronts rapidly fill the solid with interfaces, refracting light away from the camera. This process, which happens on the timescale of several seconds, can leave the resulting solid behind as an opaque structure due to the multitude of internal surfaces. This phenomenon is likely to include a phase change to the gas phase, as it can lead to a large volume increase of the final solid, which is likely from gas-filled bubbles. This behavior has been observed in rapidly freezing H_2 as well as D_2.

III.A.3. Crystal Annealing

The processes of fast crystallization and crystal growth by desublimation leave behind an opaque solid. In both cases, a subsequent annealing of the opaque crystal was observed, resulting in a fully transparent solid. Usually, the clearing starts at the bottom of the crystal and goes upward, as shown in Fig. 5. The timescale for this process for the samples in the

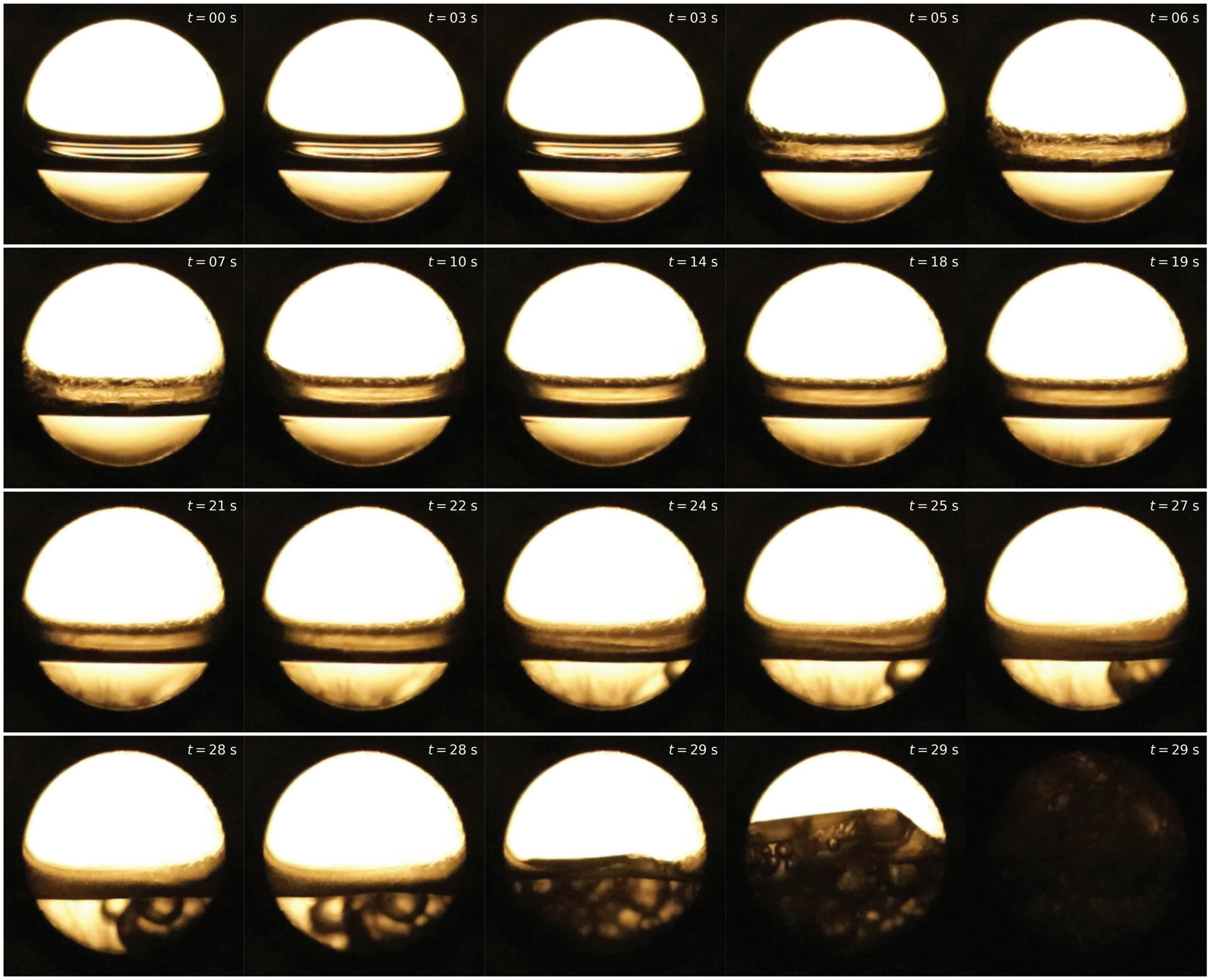

Fig. 4. Rapid freezing of liquid D_2. The cell was approximately 30% filled at the beginning of the shown process. The temperature of the cell was rapidly dropped to 14 K, and the pressure in the cell fell to 0.03 bar. The images are sequential from left to right and then top to bottom. The entire sequence of images depicts a time span of ≈30 s. Some of the processes depicted here happened very quickly, requiring several images of the cell within the span of a single second to capture the change.

T_2ApIR measurement cell was on the order of 1 day. Therefore, the annealing process not only influences the transparency of the crystal, but also its shape.

When the opaque crystal does not fill out the cell completely, the annealing leaves behind a drop-shaped clear crystal. For a homogeneous but opaque, cell-filling crystal, this shape transition is not possible. As the crystal becomes transparent only during the annealing process, the effects on the surface structure have not yet been well observed.

The parameters that influence the annealing process in the T_2ApIR measurement cell require more investigation. Presumably, the temperature in the cell, the thermal radiation through the cell windows, and the inflowing gas if the cell is still connected to the buffer vessel of the setup, have an effect. Also internal processes, like the natural ortho/para conversion in H_2 and D_2, might contribute to the annealing process.

III.B. Polariscopy to Study Stresses in Q_2 Crystals

Using back-illumination, solid Q_2 can be imaged as shown in Fig. 6. The liquid and solid phases can only be distinguished by the presence of a dark region across the phase boundary, as well as tiny imperfections in the solid. With diffused, white back-illumination from a LED, these imperfections, which consist mainly of cracks, are only faintly visible. They can be imaged much more clearly when using collimated laser light as illumination, as the

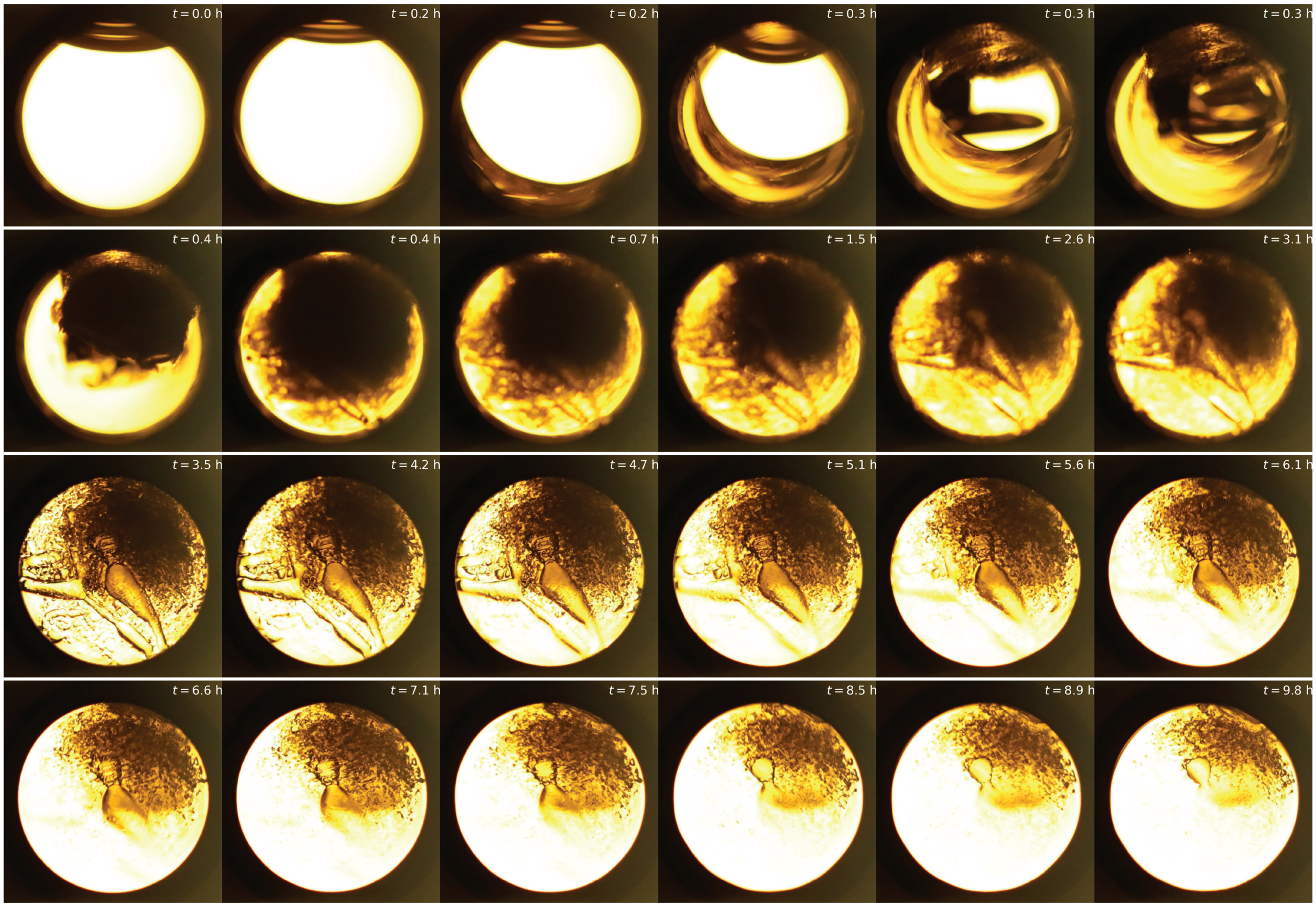

Fig. 5. Freezing and annealing of solid H_2. The cell was approximately 90% filled at the beginning of the shown process. The temperature of the cell during annealing was ≈12.5 K, and the pressure was ≈0.025 bar. The images are sequential from left to right and then top to bottom. The focus was readjusted between the second and third row. The entire sequence of images depicts a time span of ≈1 day.

stronger directionality of the light causes refractions of the light to cause a much stronger contrast.

This can be seen by comparing Figs. 6a and 6b, which show the same solid H_2, and identifying the pronounced black lines in the laser-illuminated image with the much fainter lines in the white light image. However, both of these methods provide only insights into the large-scale defects of the crystal.

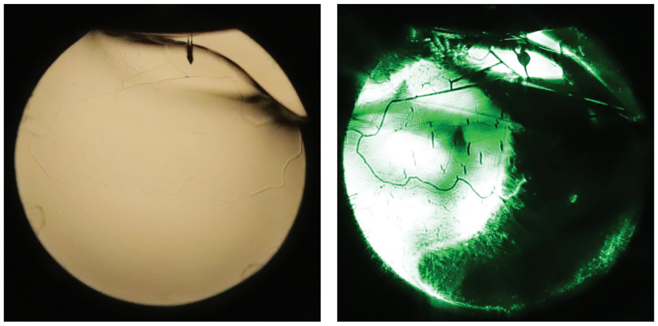

(a) LED illumination (b) Collimated 532 nm laser illumination

Fig. 6. Solid H_2 with different back-illumination. The phase boundary at the top right, as well as the cracks in the solid, slightly refract light, appearing as dark lines.

The inclusion of linear polarization filters in front of and behind the cryogenic measurement cell allows for a deeper insight into the crystal structure of the solid Q_2 to be obtained. Light transmitted through the solid Q_2, which experiences anisotropic stress, becomes optically active and causes a wavelength-dependent rotation of the polarization plane via circular birefringence [35].

For white light illumination, this rotation of the polarization plane causes areas of different stress to appear as a different color, which can be seen in Figs. 7a and 7b, where the same H_2 crystal as in Fig. 6 is shown with two different relative orientations of the polarizers around the cell. Distinct regions with sharp borders can be identified, potentially indicating a polycrystalline structure of the solid.

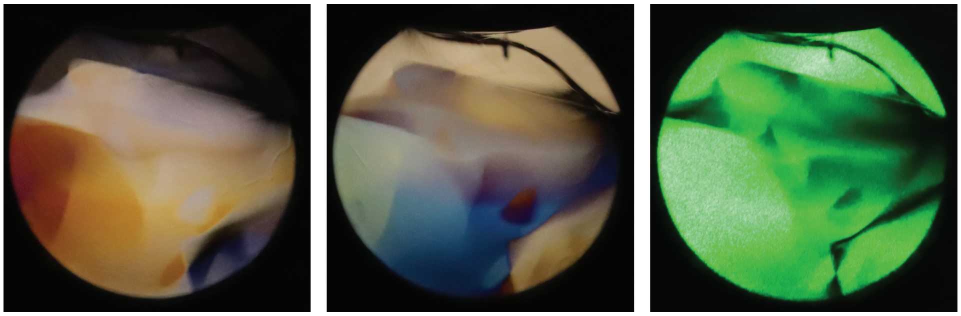

(a) LED illumination
Polarization filter setting 1

(b) LED illumination
Polarization filter setting 2

(c) Diffuse laser illumination
Polarization filter setting 2

Fig. 7. The same solid H_2 as shown in Fig. 6 but with polarization filters inserted before and after the measurement cell.

For maximal contrast, monochromatic laser back-illumination can be used; in our case, with a 532-nm diode–pumped, solid-state laser, which is shown in Fig. 7c, allowing for an easier assignment of different zones in the crystal compared to the color images.

While some features are visible in both the simple back-illuminated and polariscopy images, the latter show the internal structures of the crystal that could not be seen previously. A further feature of measurements using polarized light is the possibility to exclude the liquid phase to a large degree by setting the polarizers to be perpendicular, blocking all light that has not experienced circular birefringence in the solid. This can be seen in the upper right corner of Fig. 7a, where the light passing through the liquid H_2 and adjacent solid H_2 is strongly suppressed.

III.C. IR Spectroscopy of Isomer Change and Molecular Interactions

Due to the symmetry of the hydrogen molecule, its intrinsic dipole moment, as well as higher-order moments, are negligible on the scale of the T_2ApIR setup. For IR spectroscopy in the gaseous phase, much longer absorption paths are required. However, with the high densities in the liquid and solid phases, intermolecular interactions can induce transition dipole moments, enabling IR spectroscopy even with short absorption path lengths [36,37].

With regard to the interactions mentioned, three main contributions have been identified: molecule collisions, formation of Van Der Waals dimers (London dispersion interactions between polarizable molecules), and phonons due to the long-range interactions in the liquid and solid phases. Based on these interactions, a compact set of descriptors for the IR spectra is given in Ref. [38]. Since the IR spectra are driven by intermolecular interactions, the changes in intensity with density and composition (including ortho/para ratios) are highly nonlinear. Therefore, to use IR spectroscopy for quantitative analysis, an extensive calibration of the spectra is required [27,28].

In Fig. 8, IR absorption spectra taken over a time span of about 120 h of the same liquid H_2 sample are shown. Displayed is the first vibrational band. Most peaks are a superposition of multiple ro-vibrational excitations of molecules or dimers, respectively. During the spectra acquisition, the temperature in the measurement cell was kept constant, and therefore, the sample underwent no density changes or phase transitions. The variations in the intensities in the spectra, therefore, result only from the natural ortho/para conversion of the H_2. Starting from the room temperature equilibrium of 75% ortho-H_2 and 25% para-H_2 (first spectrum), the temperature-related ortho/para conversion shifts the corresponding ratio toward the para molecule.

From the spectra, it is clear that this conversion influences all the peaks with respect to intensity, line shape, and position. This applies even to the phonon peak $Q_{P:1}$, which seems to be ortho dominated, as its intensity decreases with the decreasing ortho-H_2 proportion. The same holds for the collision peak $Q_1(0)$, $Q_1(1)$ and the dimer peak of the transitions $S_0(1)Q_1(1)$ and $S_0(1)Q_1(0)$. On the other hand, the $S_0(0)Q_1(1) + S_0(0)Q_1(0)$ peak and the $S_0(0)S_1(0)$ peak are para dominated, and their intensity increases with the increasing amount of para-H_2 in the sample.

Most of the peaks are actually the superposition of multiple ro-vibrational transitions of the molecules and dimers [39]. One peak where the mentioned nonlinearity becomes directly visible is the collision-induced monomer peaks $Q_1(0)$ and $Q_1(1)$ (around $\nu = 4150 cm^{-1}$). Here, $Q_1(0)$ is the contribution from para-H_2 and $Q_1(1)$ from ortho-H_2. Due to the natural ortho/para

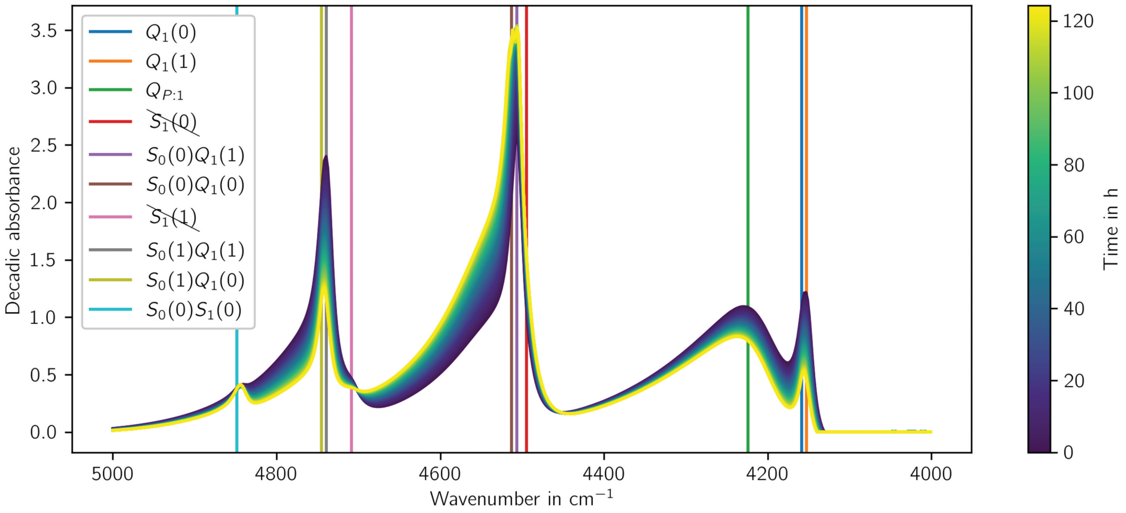

Fig. 8. IR absorption spectra of liquid H_2. Shown is the time evolution of the first vibrational band over about 120 h due to the natural ortho/para conversion. The line positions were taken from Ref. [38]. The spectra are taken with a resolution of 6.0 cm^{-1}. Each spectrum is composed of 64 scans adding up to an acquisition time of nearly 40 s.

conversion, the corresponding ratio is shifting toward the para molecule.

While the sum of the occupational numbers of the rotational states $J = 0$ and $J = 1$ is constant during the ortho-para conversion, the total intensity decreases due to differences in the molecular interaction potential. This peak is then followed by a phonon transition around $v = 4250\ \mathrm{cm}^{-1}$ (labeled $Q_{P:1}$). All the spectral features from $v = 5000$ to $4400\ \mathrm{cm}^{-1}$ are then based on dimer transitions.

Forming a comprehensive model of the line positions and intensities as a function of the isotopic and isomeric compositions is one of the core objectives of the T_2ApIR experiment. This is accomplished by referencing the composition of the cell content in situ against Raman spectroscopy, which has a well known and linear response to the different hydrogen isotopologues and isomers.

III.D. Raman Spectroscopy of Isotopic and Isomer Composition

The Raman setup of the T_2ApIR experiment allows for the spectroscopy of the cryogenic cell contents. As mentioned in Sec. II, two different spectrometers can be connected to the collection side, which allows for the investigation of either the S_0-branch (rotational) or the Q_1-branch (ro-vibrational) of the hydrogen isotopologues.

For the S_0-branch, the range of the wavenumbers that needs to be covered spans between the $S_0(0)$ peak of T_2 at 120 cm^{-1} on the lower end up to at least the $S_0(4)$ peak of H_2 at 1246 cm^{-1}. Higher rotational states J are not significantly occupied at temperatures that can be reached with T_2ApIR.

For the Q_1-branch, the range of the wavenumbers that needs to be covered spans between the $Q_1(0)$ peak of T_2 at 2464 cm^{-1} on the lower end up to at least the $Q_1(0)$ peak of H_2 at 4161 cm^{-1}. Example spectra for both cases are shown in Fig. 9.

In the S_0-branch shown in Fig. 9a, one can clearly see both the $S_0(0)$ line originating from para-H_2 at 354 cm^{-1} and the $S_0(1)$ line from ortho-H_2 at 587 cm^{-1}. Besides these lines, some additional Raman lines at 417 cm^{-1} and 751 cm^{-1} resulting from the sapphire windows [40] are visible. As these lines are comparatively low and constant in intensity, they can be subtracted.

In the Q_1-branch shown in Fig. 9b, an overlapping line from the H_2 $Q_1(0)$ and $Q_1(1)$ lines is visible at ≈4160 cm^{-1}. Furthermore, the $S_1(0)$ line of the S_1-branch at 4498 cm^{-1} can be seen in between a multitude of other lines. These background lines are not Raman lines, but photoluminescence of the chromium impurities in the sapphire windows, which get excited by the incident laser light.

The photoluminescence lines do not not interfere significantly with the Q_1-branch of H_2, which has the highest Raman shift of all isotopologues. However, as they can cause detector saturation and limit the maximal acquisition time, these lines will be removed using a short-pass filter in the future when necessary.

Due to the much higher densities at low temperatures, and especially in the liquid phase or solid phase,

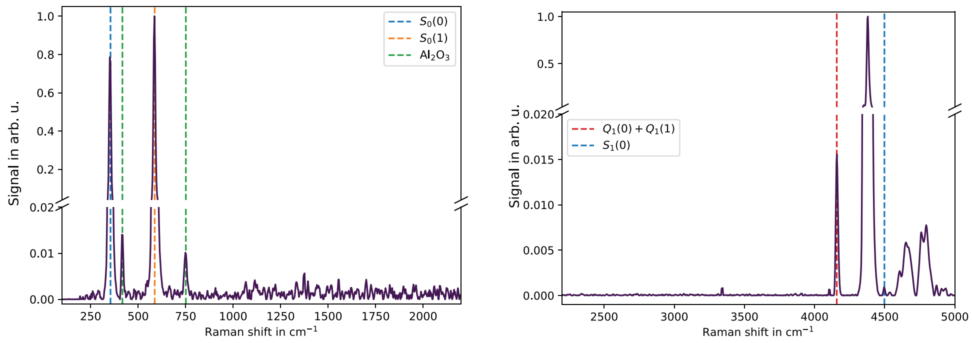

(a) S_0-branch region
Acquisition time of 60 s

(b) Q_1-branch region
Acquisition time of 5 s

Fig. 9. Sample Raman spectra of liquid H_2. Some background peaks are labeled for reference.

a much stronger Raman signal than in the gas phase at room temperature was observed. As a result, the measurement times can be drastically decreased, providing access to dynamic processes on the timescale of seconds.

An example of this is the condensation of liquid H_2 into the measurement cell, which is shown in Fig. 10. At first, only the signal of H_2 in the gas phase is visible, which increases in density as the gas cools down. Then condensation happens, and at around the 350-s mark, the level of the condensed liquid rises into the laser beam path. Up until around 490 s, the filling level of the cell rises, until all available gas down to the saturation curve has been condensed. In this example the filling level never covered the entire laser beam cross section.

Based on the different S_0-branch Raman lines of the hydrogen isotopologues, a monitoring of the ortho/para spin isomer state is possible. This is done by integrating the peak areas for all the $S_0(J)$ peaks individually, weighting these areas with the transition matrix elements of the different transitions, and then summing up the even J peaks for the para and the odd J peaks for the ortho state.

At the temperatures where hydrogen is in the liquid phase, states with $J \geq 2$ are not significantly occupied ($<10^{-6}$ at 33 K), therefore only the $S_0(0)$ and $S_0(1)$ peaks

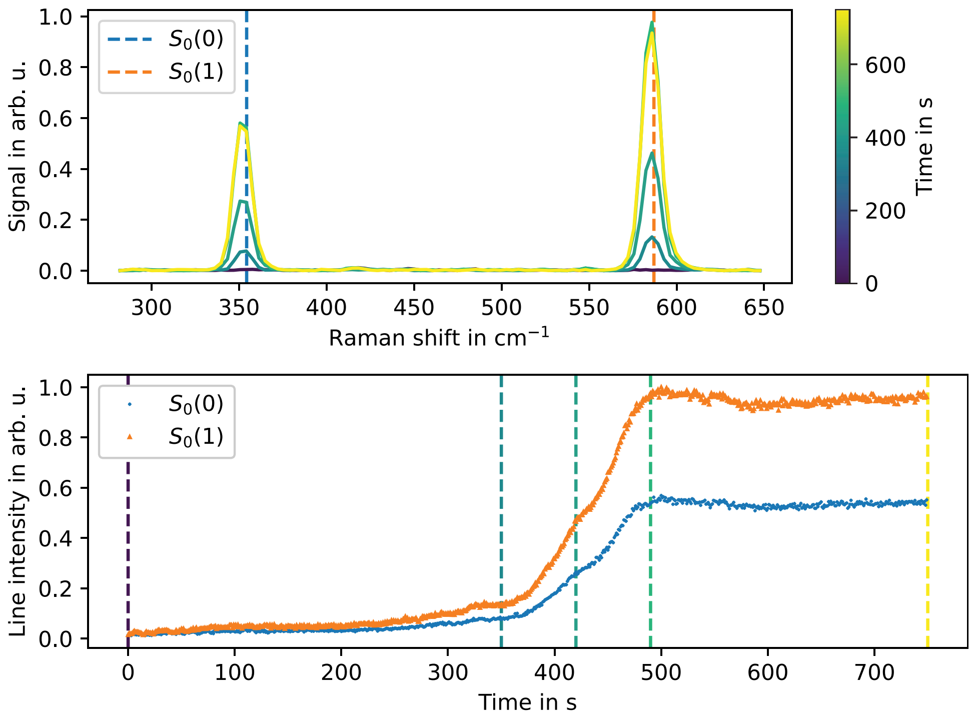

Fig. 10. Raman spectra and line intensity as function of time for H_2 condensing into the measurement cell. The spectra were acquired with an integration time of 1 s each.

are present (as can be seen in Fig. 9a), and monitoring them is sufficient in order to determine the ortho/para ratio. An example of this is shown in Fig. 11, where H_2 with a room temperature equilibrium ortho/para ratio of $\approx 75/25$ was condensed into the measurement cell. The high densities in the liquid phase caused a gradual conversion from the ortho to the para state, which is the preferred state at low temperatures, at much higher rates than in the gas phase.

The ortho/para ratio measured in the cell will be calibrated against an external reference laser Raman system at room temperature to ensure accurate measurements of the chemical and spin isomer composition. However, being able to monitor the ortho/para ratio in situ will allow for a direct cross calibration of the IR spectra of the liquid or solid phases without the need to evaporate the sample into a room temperature measurement setup.

In particular, for layered mixtures of liquids or solids where the effects of diffusion can be of interest, this has the crucial advantage of preserving the layered structure as the Raman spectrum measurement is performed.

IV. CONCLUSION AND OUTLOOK

The T_2ApIR experiment aims to investigate the properties of all six hydrogen isotopologues, their spin isomers, and their mixtures in the gaseous, liquid, and solid phases, as well as the dynamics of their phase changes. These investigations will be primarily performed using optical methods, including polariscopy as well as IR and Raman spectroscopy. Commissioning measurements have been performed to verify the different methods.

In this paper, it has been demonstrated that both IR and Raman spectroscopy can be used to obtain in situ information about the isotopic and isomer concentrations of hydrogen isotpologues in the T_2ApIR setup. The higher density in the liquid phase compared to the gas phase allows for short acquisition times, enabling real-time monitoring of the compositions, showing the potential of both of the spectroscopic methods.

In addition to the spectroscopic methods, the option to image the cell contents allows for the unambiguous attribution of spectroscopic information to different phases, ensuring the correct interpretation of spectral data. The performed polariscopy measurements have demonstrated the capability to reveal additional information regarding the crystallization of H_2 and D_2.

Based on the experience obtained during the scientific commissioning phase with the inactive hydrogen isotopologues, further research will cover several different topics.

With further development, the spectroscopic methods will be refined into useful tools for process optimization and monitoring in applications using liquid hydrogen, such as the fundamental experimental physics, the hydrogen economy, or the fusion fuel cycle. A key factor for this, and a focus of the upcoming activities of the T_2ApIR experiment, will be calibrating these in situ measurement methods against each other and against an external reference.

Based on the observations obtained for the crystal formation, different procedures to grow crystals of

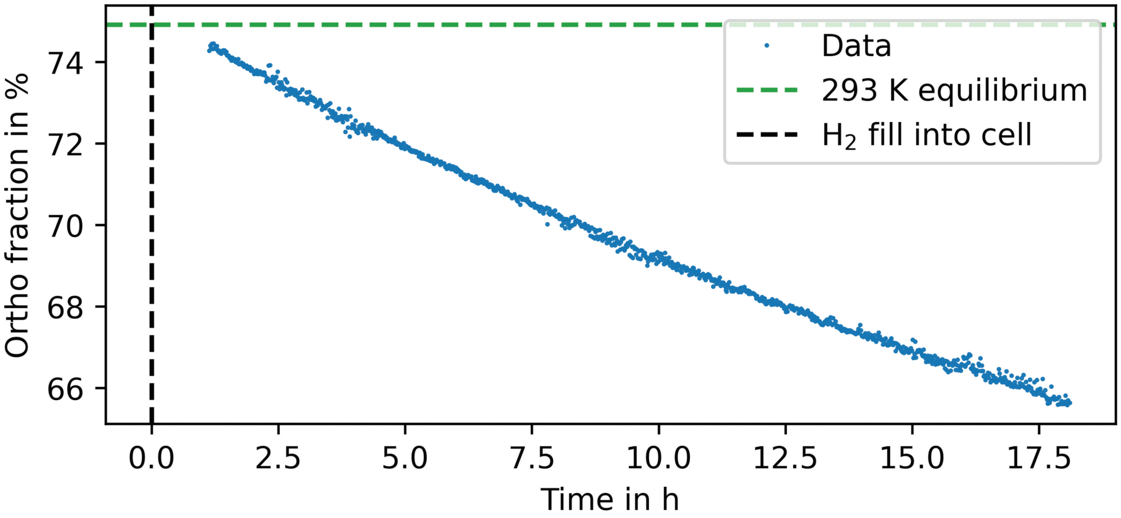

Fig. 11. Evolution of ortho fraction of liquid H_2, condensed from the room temperature equilibrium ortho/para ratio, due to natural conversion in the liquid phase. Shown are calculated from raw data using only background subtraction and theoretical line strengths. The spectra used for this calculation were acquired with an integration time of 60 s each.

hydrogen isotopologues and their mixtures will be investigated, with the aim to find a scalable, repeatable, and fast way of creating homogeneous crystals, which will be needed for the production of fuel pellets for magnetic confinement fusion or targets for inertial confinement fusion.

Combining both imaging and spectroscopic measurements will allow for the investigation of effects such as the diffusion of hydrogen isotopologues or isomers into each other in layered systems.

After successfully commissioning the analytical systems with the inactive hydrogen isotopologues, T_2ApIR will be transitioned to tritium operations. Following a measurement phase focusing on burn-in effects during commissioning, measurement phases focusing on the spectroscopy of the hydrogen isotopologues in different phases, as well as on the crystallization behavior of pure tritium and tritium-containing mixtures, will follow.

On a longer timescale, an upgrade of the IR detection system is planned, replacing the single-pixel detector with a two-dimensional focal plane array to achieve hyperspectral imaging in the IR range. Such an analytic system can potentially be used to investigate the isotopic distribution of deuterium and tritium within fuel pellets or inertial fusion targets.

Author Contributions

CRediT: **Alexander Marsteller:** Data curation, Formal analysis, Funding acquisition, Investigation, Methodology, Project administration, Software, Supervision, Validation, Visualization, Writing – original draft, Writing – review & editing; **Dominic Batzler:** Formal analysis, Investigation, Supervision, Visualization; **Beate Bornschein:** Conceptualization, Funding acquisition, Project administration, Writing – original draft, Writing – review & editing; **Lutz Bornschein:** Investigation, Methodology, Project administration, Resources, Supervision, Writing – review & editing; **Elisabeth Eckard:** Formal analysis, Investigation; **Florian Hanß:** Methodology, Project administration, Resources, Writing – review & editing; **Joshua Kohpeiß:** Methodology, Project administration, Supervision, Writing – review & editing; **Daniel Kurz:** Data curation, Formal analysis, Investigation, Supervision, Validation, Writing – original draft, Writing – review & editing; **Ralph Lietzow:** Methodology, Project administration, Supervision, Writing – review & editing; **Michael Sturm:** Conceptualization, Methodology, Project administration, Resources, Supervision, Writing – review & editing; **Tin Vrkic:** Formal analysis, Investigation; **Stefan Welte:** Methodology, Project administration, Resources, Writing – review & editing; **Robin Größle:** Conceptualization, Funding acquisition, Investigation, Project administration, Resources, Supervision, Visualization, Writing – original draft, Writing – review & editing.

Disclosure Statement

No potential conflict of interest was reported by the author(s).

Funding

This work was partially supported by the Bundesministerium für Forschung, Technologie und Raumfahrt (German Federal Ministry of Research, Technology and Space) within the Verbundprojekt: Inertial Fusion Energy (IFE) Targetry HUB für die DT-Trägheitsfusion - Teilvorhaben: Tritium-Phasenraum-Navigation provided under grant number [13F1013H].

ORCID

Alexander Marsteller http://orcid.org/0000-0002-9620-4512
Dominic Batzler http://orcid.org/0009-0008-9040-9104
Beate Bornschein http://orcid.org/0000-0002-2930-8549
Lutz Bornschein http://orcid.org/0000-0003-4483-0471
Michael Sturm http://orcid.org/0000-0003-0479-3258
Stefan Welte http://orcid.org/0000-0002-0678-9845

References

1. B. Bornschein, "Determination of Neutrino Mass from Tritium Beta Decay," *Fusion Sci. Technol.*, **54**, *1*, 59 (2008); https://doi.org/10.13182/fst54-59.
2. M. Sturm et al., "Kilogram Scale Throughput Performance of the KATRIN Tritium Handling System," *Fusion Eng. Des.*, **170**, 112507 (2021); https://doi.org/10.1016/j.fusengdes.2021.112507.
3. M. Aker et al., "Direct Neutrino-Mass Measurement Based on 259 Days of KATRIN Data," *Science*, **388**, *6743*, 180 (2025); https://doi.org/10.1126/science.adq9592.
4. A. A. Esfahani et al., "Determining the Neutrino Mass with Cyclotron Radiation Emission Spectroscopy—Project 8," *J. Phys. G: Nucl. Part. Phys.*, **44**, *5*, 054004 (2017); https://doi.org/10.1088/1361-6471/aa5b4f.
5. A. A. S. Amad et al., "Determining Absolute Neutrino Mass Using Quantum Technologies," *New J. Phys.*, **27**, *10*, 105006 (2025); https://doi.org/10.1088/1367-2630/adc624.
6. E. Aprile et al., "Excess Electronic Recoil Events in XENON1T," *Phys. Rev. D.*, **102**, *7*, 072004 (2020); https://doi.org/10.1103/physrevd.102.072004.
7. Y. Meng et al., "Dark Matter Search Results from the PandaX-4T Commissioning Run," *Phys. Rev. Lett.*, **127**,

26, 261802 (2021); https://doi.org/10.1103/physrevlett.127.261802.

8. M. Adrover et al., "Cosmogenic Background Simulations for Neutrinoless Double Beta Decay with the DARWIN Observatory at Various Underground Sites," *Eur. Phys. J. C.*, **84**, 88 (2024); https://doi.org/10.1140/epjc/s10052-023-12298-w.
9. I. Arnquist et al., "Exotic Dark Matter Search With the MAJORANA Demonstrator," *Phys. Rev. Lett.*, **132**, *4*, 041001 (2024); https://doi.org/10.1103/physrevlett.132.041001.
10. J. Aalbers et al., "Dark Matter Search Results from 4.2 Tonne-Years of Exposure of the LUX-ZEPLIN (LZ) Experiment," *Phys. Rev. Lett.*, **135**, 011802 (2025); https://doi.org/10.1103/4dyc-z8zf.
11. *Fundamentals of Magnetic Fusion Technology*, G. Van Oost, Ed. International Atomic Energy Agency, Vienna, Austria (2023); https://www.iaea.org/publications/14898/fundamentals-of-magnetic-fusion-technology.
12. J. Wydra et al., "ViMA —The Spinning Rotor Gauge to Measure the Viscosity of Tritium Between 77 and 300 K," *Fusion Sci. Technol.*, **80**, *3–4*, 616 (2023); https://doi.org/10.1080/15361055.2023.2238170.
13. B. Krasch et al., "Raman Spectroscopy for Ortho-Para Hydrogen Catalyst Studies," *Int. J. Hydrogen Energy*, **48**, *77*, 29952 (2023); https://doi.org/10.1016/j.ijhydene.2023.03.461.
14. G. Bison et al., "Temperature-Dependent Ultracold Neutron Transmission in $^2H_2$ Gas: A Test of the Young-Koppel Model," *Phys. Rev. C.*, **112**, 014007 (2025); https://doi.org/10.1103/1r5v-6h9p.
15. S. Niemes and J. R. Braun, "Speed of Sound Measurement of Hydrogen Isotopologues Containing Tritium for Reference Gas Sample Verification," *Fusion Sci. Technol.*, **80**, *3–4*, 558 (2023); https://doi.org/10.1080/15361055.2023.2209087.
16. F. Priester et al., "A New Facility for the Measurement of the Sieverts'-Constant for PbLi with Tritium," *Fusion Eng. Des.*, **191**, 113568 (2023); https://doi.org/10.1016/j.fusengdes.2023.113568.
17. J. M. Wydra, "First Measurement of the Tritium Viscosity in a Temperature Range from 100 K to 300 K," Ph.D. Thesis, Institute for Astroparticle Physics (IAP) and Institute for Experimental Particle Physics (ETP), Karlsruhe Institute of Technology (2025); https://doi.org/10.5445/IR/1000178925.
18. F. Priester et al., "μRA—A New Compact Easy-to-Use Raman System for All Hydrogen Isotopologues," *Sensors*, **22**, *10*, 3952 (2022); https://doi.org/10.3390/s22103952.
19. S. Niemes et al., "Accurate Reference Gas Mixtures Containing Tritiated Molecules: Their Production and Raman-Based Analysis," *Sensors*, **21**, *18*, 6170 (2021); https://doi.org/10.3390/s21186170.
20. M. Aker et al., "Quantitative Long-Term Monitoring of the Circulating Gases in the KATRIN Experiment Using Raman Spectroscopy," *Sensors*, **20**, *17*, 4827 (2020); https://doi.org/10.3390/s20174827.
21. M. Sturm et al., "Monitoring of All Hydrogen Isotopologues at Tritium Laboratory Karlsruhe Using Raman Spectroscopy," *Laser Phys.*, **20**, *2*, 493 (2009); https://doi.org/10.1134/s1054660x10030163.
22. F. Priester, "A New Device for Activity Measurement of Tritiated Water," *Fusion Sci. Technol.*, **71**, *4*, 600 (2017); https://doi.org/10.1080/15361055.2017.1289585.
23. I. Cristescu et al., "Review of the TLK Activities Related to Water Detritiation, Isotope Separation Based on Cryogenic Distillation and Development of Barriers Against Tritium Permeation," *Fusion Sci. Technol.*, **71**, *3*, 225 (2017); https://doi.org/10.1080/15361055.2017.1288057.
24. P. C. Souers, *Hydrogen Properties for Fusion Energy*, University of California Press, Oakland, CA (1986); https://doi.org/10.1525/9780520338401.
25. R. Lässer and S. Grünhagen, "Gas Chromatography at the Tritium Laboratory Karlsruhe," Eggenstein-Leopoldshafen, Germany: Forschungszentrum Karlsruhe (2003); https://doi.org/10.5445/IR/270055409.
26. S. G. Romanelli et al., "Upgraded Analytical Gas Composition Technique in the Tritium Fuel Cycle of JET," *Fusion Sci. Technol.*, **71**, *4*, 467 (2017); https://doi.org/10.1080/15361055.2017.1293432.
27. R. Größle et al., "First Calibration of an IR Absorption Spectroscopy System for the Measurement of H_2, D_2, and HD Concentration in the Liquid Phase," *Fusion Sci. Technol.*, **71**, *3*, 369 (2017); https://doi.org/10.1080/15361055.2017.1291237.
28. S. Mirz et al., "Concentrated Nonequilibrium HD for the Cross Calibration of Hydrogen Isotopologue Analytics," *Fusion Sci. Technol.*, **76**, *3*, 284 (2020); https://doi.org/10.1080/15361055.2020.1711688.
29. O. A. Hurricane, "Inertial Confinement Fusion: Status and Challenges," *Annu. Rev. Nucl. Part. Sci.*, **75**, *1*, 153 (2025); https://doi.org/10.1146/annurev-nucl-102622-022842.
30. D. T. Goodin et al., "Developing a Commercial Production Process for 500 000 Targets per Day: A Key Challenge for Inertial Fusion Energy," *Phys. Plasmas*, **13**, *5* (2006); https://doi.org/10.1063/1.2177129.
31. R. Größle et al., "First Calibration Measurements of an FTIR Absorption Spectroscopy System for Liquid Hydrogen Isotopologues for the Isotope Separation System of Fusion Power Plants," *Fusion Sci. Technol.*, **67**, *2*, 357 (2015); https://doi.org/10.13182/fst14-t29.
32. B. Krasch et al., "Design of a Cryostat for Spectroscopic Investigation of All Hydrogen Isotopologues in the Solid,

Liquid, and Gaseous Phases," *Fusion Sci. Technol.*, **76**, *4*, 481 (2020); https://doi.org/10.1080/15361055.2020.1718841.

33. J. Kohpeiß et al., "Commissioning of an Experiment for Thermodynamic and Spectroscopic Studies of Hydrogen Isotopologues at Cryogenic Conditions," *arXiv Preprint arXiv: arXiv:2512.08788* (2025); https://doi.org/10.48550/ARXIV.2512.08788.
34. S. Welte et al., "Tritium Laboratory Karlsruhe: Administrative and Technical Framework for Isotope Laboratory Operation," *Fusion Sci. Technol.*, **67**, *3*, 635 (2015); https://doi.org/10.13182/fst14-t98.
35. N. N. Zholonko, "Chromatic Polarization in Solid Parahydrogen with an Argon Impurity at an Extremely Low Concentration," *Phys. Solid State*, **53**, *1*, 138 (2011); https://doi.org/10.1134/s1063783411010379.
36. A. R. W. McKellar, "Possible Identification of Sharp Features in the Voyager Far-Infrared Spectra of Jupiter and Saturn," *Can. J. Phys.*, **62**, *8*, 760 (1984); https://doi.org/10.1139/p84-104.
37. A. R. W. McKellar, "Experimental Verification of Hydrogen Dimers in the Atmospheres of Jupiter and Saturn from Voyager IRIS Far-Infrared Spectra," *Astrophys. J.*, **326**, L75 (1988); https://doi.org/10.1086/185126.
38. R. Grössle et al., "Minimal and Complete Set of Descriptors for IR-Absorption Spectra of Liquid H2–D2 Mixtures," *AIP Adv.*, **10**, 055108 (2020); https://doi.org/10.1063/1.5111000.
39. M. Gustafsson, L. N. Fletcher, and G. S. Orton, "A Computational Study of Hydrogen Dimers in Giant-Planet Infrared Spectra," *J. Phys. Conf. Ser.*, **1289**, *1*, 012010 (2019); https://doi.org/10.1088/1742-6596/1289/1/012010.
40. A. Bellafatto and I. E. Reimanis, "Three-Dimensional Spectral and Spatial Resolution of Raman Measurements in Sapphire," *J. Am. Ceram. Soc.*, **108**, *12*, e70202 (2025); https://doi.org/10.1111/jace.70202.